Flight control system design with $\mathcal{H}_\infty$ loop-shaping approach through non-diagonal weights

R. Panesi and G. Mengali
g.mengali@ing.unipi.it
Department of Aerospace Engineering
University of Pisa
Pisa, Italy

ABSTRACT

This paper deals with the design methodology of multi-variable flight control systems through a $\mathcal{H}_\infty$ loop-shaping technique. A new procedure for the design of non-diagonal pre-and post-compensators is described. In particular, important improvements over existing methods are introduced to both make the selection of weights easier and to contain the order of the resulting controller. The new procedure can be easily managed through suitable Matlab commands and functions, thus simplifying the whole algorithm implementation and providing an effective control system design with a minimum effort. Two typical design problems are addressed: a pitch pointing control system and a lateral controller for coordinated turns. In both cases, a good decoupling between existing channels is obtained by means of a non-diagonal pre-compensator which shapes the plant transfer function, and provides the desired response settling time. The design approach is particularly effective even for nominal plants with strong cross-coupling between channels. The design procedure is illustrated with the aid of a Matlab/Simulink model of a single seat fighter aircraft. We show that a trade-off between the conflicting requirements of fast response and moderate use of control surfaces can be easily managed by varying the constant terms of the diagonal post-compensator.

NOMENCLATURE

$\mathbf{A}$	state matrix
$\mathbf{B}$	input matrix
$\mathbf{C}$	output matrix
$\mathbf{D}$	feedforward matrix
$\underline{D}$	$\mathbf{D}^{\mathrm{T}}\mathbf{D}$
$F(s)$	spectral factor of ψ^T
$G(s)$	plant transfer function
$G_s(s)$	plant transfer function after shaping
$\mathbf{H}$	Hamiltonian matrix
$\mathbf{I}$	identity matrix
K(s)	overall controller
K_∞(s)	feedback $\mathcal{H}_\infty$ controller
M	Mach number
$\mathbf{U}(s)$	matrix of left singular vectors of G
$\mathbf{U}_{\mathbf{GW}_1}(s)$	matrix of left singular vectors of GW_1
$\mathbf{V}(s)$	matrix of right singular vectors of G
$\mathbf{V}_{\mathbf{GW_1}}(s)$	matrix of right singular vectors of GW_1
$\mathbf{W}(s)$	diagonal weighting matrix that shapes $\sum$
$\mathbf{W}_1(s)$	pre-compensator
$\mathbf{W}_{1_r}(s)$	reduced order pre-compensator
$\mathbf{W}_2(s)$	post-compensator
$\boldsymbol{X}$	matrix, solution of Riccati equation

Paper No. 3358. Manuscript received 14 October 2008, revised version received 12 March 2009 accepted 30 March 2009.

https://doi.org/10.1017/S0001924000003110 Published online by Cambridge University Press

$f_i(s)$	transfer function, entry of W
h	flight altitude
j	imaginary unit
p	roll rate
q	pitch rate
r	yaw rate
t	time
$\mathbf{u}$	input vector
w_1	shaped plant input disturbance
w_2	shaped plant output disturbance
$\mathbf{x}$	state vector
z_1	controller output
z_2	controller input
$\Gamma(s)$	transfer matrix that shapes $\sum$ reflecting the conditioning of W_1
$\Pi(s)$	transfer matrix that shapes $\sum$ reflecting the conditioning of W_2
$\sum(s)$	matrix containing singular values of G
$\sum_s(s)$	matrix containing shaped singular values
$\sum_{GW_1}(s)$	matrix containing singular values of GW_1
$\psi(s)$	auxiliary matrix, see Equation (7)
α	incidence angle
β	sideslip angle
$\gamma_i(s)$	generic entry of Γ
γ	flight path angle
$\bar{\gamma}$	robust stability margin
δ	indicator to verify how $\hat{V}$ fits V
δ_c	actuated canard deflection
δ_{c_c}	commanded canard deflection
δ_e	actuated elevon deflection
δ_{e_c}	commanded elevon deflection
δ_r	actuated rudder deflection
δ_{r_c}	commanded rudder deflection
θ	pitch attitude angle
$\pi_i(s)$	generic entry of Π
σ_i	singular value, entry of the matrix $\sum$
$\bar{\sigma}$	maximum singular value
$\underline{\sigma}$	minimum singular value
ω	frequency
ω_L	lower limit of frequency range
ω_H	upper limit of frequency range
ϕ	roll attitude angle
$\mathcal{A}$	matrix, coefficient of Riccati equation
$\mathcal{Q}$	matrix, coefficient of Riccati equation
$\mathcal{R}$	matrix, coefficient of Riccati equation

Subscripts

i, j	indexes (row,column) of a matrix entry
–	spectral factor of a transfer matrix

Superscripts

T	transpose
*	conjugate transpose
~	pertransposed system, $H^{\sim}(s) \triangleq H(-s)^{\mathrm{T}}$
^	approximating matrix

1.0 INTRODUCTION

Among the existing methods for designing robust multi-variable control systems, the loop-shaping design with $\mathcal{H}_\infty$ controller synthesis plays a role of primary importance. The original source of this approach can be dated back in 1990 with the work by McFarlane and Glover[1]. Subsequently, it has been the subject of considerable developments and applications especially in the aerospace field. An excellent description of its peculiarities can be found, for example, in Ref. 2.

Basically, the methodology consists in a two-stage design process[3,4]: first, the desired closed-loop performance is achieved by applying a pre-compensator $\mathbf{W}_1$ and a post-compensator $\mathbf{W}_2$ to the nominal plant G[†]. These two compensators are chosen in such a way that the singular values of the shaped plant satisfy the design requirements. Usually, the loop gain is desired to be high at low frequencies (that is, in the bandwidth region), low at high frequencies and with a 'gentle' slope (equal to –20dB/decade) in the crossover region. A commonly used set-up of the loop-shaping block diagram[2] is shown in Fig. 1.

When the weighted plant $G_S \triangleq \mathbf{W}_2 G \mathbf{W}_1$ is robustly stabilised with respect to coprime factor uncertainties (the most general type of unstructured uncertainty), the controller K_∞ is obtained as the output of the design procedure. In essence, the ∞-norm of the transfer matrix from the disturbances at the output and input of the shaped plant, to the controller output and input, is minimised over all stabilising controllers, that is:

$$\inf_{\text{stab } K_\infty} \left\| \begin{bmatrix} K_\infty \\ I \end{bmatrix} (I - G_S K_\infty)^{-1} \begin{bmatrix} I & G_S \end{bmatrix} \right\|_\infty = \bar{\gamma} \qquad \ldots (1)$$

where $\bar{\gamma}$ defines the stability margin for the robust stability problem. In other terms, $\bar{\gamma}$ is a measure of how robust the shaped plant is with respect to perturbations (in terms of coprime factorisation of the plant).

If the robust stabilisation is successful, that is, if $\bar{\gamma}$ is not too large, the shape of the singular values of the robustly stabilised plant is known to be similar to that of the open-loop shaped plant[5]. A value of $\bar{\gamma} < 4$ is known to be representative of a satisfactory design, based on both theoretical arguments[4] and common practice[6]. The overall controller is, therefore, given by $\mathbf{K} = \mathbf{W}_1 \mathbf{K}_\infty \mathbf{W}_2$.

The classical and well established procedure for $\mathcal{H}_\infty$ loop-shaping design has been developed by Hyde[6]. It is a step-by-step procedure, helpful in the definition of the weighting matrices $\mathbf{W}_1$ and $\mathbf{W}_2$ that are typically chosen as diagonal. While the choice of diagonal weights is rather simple and effective in many cases, there exist situations of practical interest in which Hyde's procedure fails. This problem is especially important for plants with highly coupled dynamics, since it involves a frustrating trial and error approach and does not guarantee that the selected diagonal weights provide the desired loop shape to the plant. A typical example of such a situation is given by the lateral dynamics of an aircraft. In particular, when the designer is asked to align the singular values of the shaped plant at a desired frequency (usually, at the required bandwidth), the use of non-diagonal terms in the weighting functions cannot, in practice, be avoided.

A procedure for the design of non-diagonal pre- and post-compensators has been developed by Papageorgiou and Glover[7]. In essence, the designer is enabled to shape each singular value of the nominal plant separately, in such a way that the desired loop shape can be eventually achieved[7]. The resulting weighting matrices are stable and minimum phase.

This paper introduces some improvements to the approach by Papageorgiou and Glover, with particular emphasis to the design implementation in the aerospace field. In particular, two problems concerning the multi-variable design of flight control laws are discussed, that is, the design of a pitch pointing control system and a lateral controller for coordinated turns.

The paper is organised as follows. The proposed step-by-step design methodology is reviewed, and additions/improvements with respect to the original procedure by Papageorgiou and Glover are discussed. Each step can be easily managed through suitable Matlab commands and functions, thus simplifying the whole algorithm implementation and providing an effective control system design with a minimum effort. Two case studies are fully described and some practical conclusions are emphasised.

[†] The Laplace variable s is often omitted for simplicity. Matrices that depend on s are emphasised in the nomenclature.

https://doi.org/10.1017/S0001924000003110 Published online by Cambridge University Press

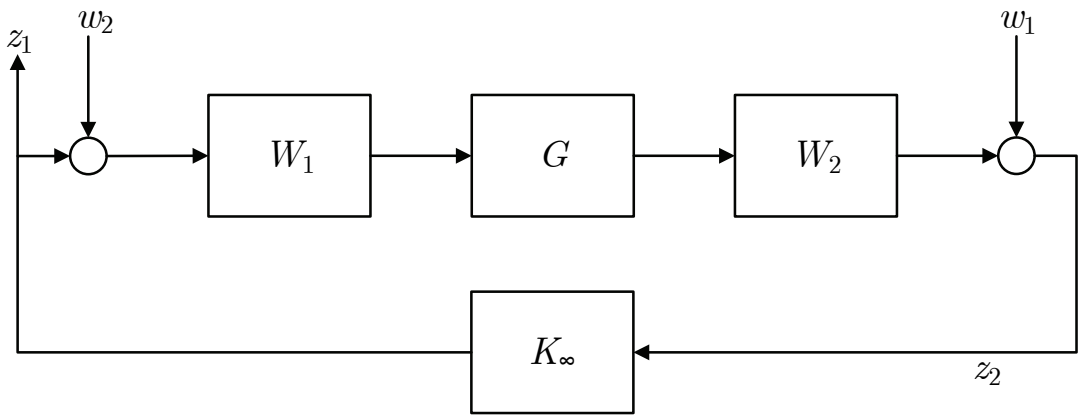


Figure 1. Implementation for a loop-shaping controller.

2.0 DESIGN METHODOLOGY

As stated, the proposed step-by-step design methodology is a revision of the approach by Papageorgiou and Glover[7]. A first important improvement consists in the fact that most steps of the original procedure have been automated, thus substantially reducing the effort required by the designer in the controller synthesis. Another interesting feature is the introduction of additional aids, aiming to reduce the order of the resulting weighting matrices and of the overall controller. This reduction is necessary because in most cases the design procedure generates weighting matrices with a high number of states. To simplify the designer's job, the whole procedure has been implemented in a straightforward way through a Matlab routine. Accordingly, the only work which is required in practice is the choice of the matrix that reflects the desired conditioning of the pre-compensator (step 4 of the procedure). All other activities are performed automatically.

To begin, consider a linear time-invariant plant model G, with m inputs and n outputs and with no poles or zeros on the imaginary axis. Without loss of generality, and to simplify our notation, assume that G is square, that is, $n = m$. Assume that G is the scaled plant: indeed, it is a common practice to scale both plant inputs and outputs before the shaping activity. This is done to improve the model conditioning and to make the selection of weights easier. The whole project methodology can be summarised in the following points.

1. Select a suitable frequency range $[\omega_L.\omega_H]$ and grid it, thus obtaining a vector whose entries are sufficiently representative values of frequency ω. In particular, the interval $[\omega_L.\omega_H]$ must contain all the dynamics of interest of G.
2. Perform a singular value decomposition of the plant transfer matrix $G(j\omega)$ per frequency value of ω in the grid, that is;

$$G(j\omega) = U(j\omega)\Sigma(j\omega)V(j\omega)^* \quad \ldots (2)$$

3. A transfer matrix $\hat{\mathbf{V}}$ must now be found whose generic entry $\hat{v}_{ij}$ should fit the corresponding entry v_{ij} of $\mathbf{V}$. This is a crucial point because the design success of the shaped plant is heavily dependent on the effectiveness with which $\hat{\mathbf{V}}$ approximates $\mathbf{V}$ as a function of ω. This step constitutes a major improvement with respect to the original procedure by Papageorgiou and Glover[7] because the best choice of $\mathbf{V}$ has now been automated. This result is possible by means of the capabilities of existing software. In fact Matlab offers a number of functions and commands for building transfer functions capable of approximating the frequency response of a system. In this process the designer is only asked to specify the order of the approximating transfer function. In our case, each vector, whose entries are the magnitudes given by v_{ij} (with $i, j = 1,...,m$) per each value of ω, is built separately. More precisely, the proposed algorithm begins by approximating v_{ij} through a first order transfer function. Then, an iterative cycle generates transfer functions of increasing order until the following inequality is met:

$$|\hat{v}_{ij}(j\omega)| - |v_{ij}(j\omega)| \le \delta, \quad \forall \omega. \quad \ldots (3)$$

Note that δ (which is specified by the user) is a direct measure of the approximation degree. Indeed, the smaller the value of δ, the better the fit is.

4. The desired loop shape, that is, the singular values of the weighted plant, has now to be found. To do this, each singular value of G, σ_i (where $i = 1,...,m$), is weighted through a transfer function f_i, chosen by the designer upon his/her experience and taking into account the design requirements. Note that both f_i and f_i^{-1} are minimum phase and stable, that is, $f_i, f_i^{-1} \in \mathcal{RH}_\infty$

Consider the diagonal matrix $W \triangleq diag(f_1,\ldots,f_m)$. Papageorgiou and Glover[7] suggest that $\mathbf{W}$ is split in two matrices Π and Γ, such that $\mathbf{W} = \Pi\Gamma$. Note that $\Pi = diag(\pi_1,\ldots,\pi_m)$ and $\Gamma = \mathrm{diag}(\gamma_1,\ldots,\gamma_m)$ are chosen to reflect the conditioning of $\mathbf{W}_2$ and $\mathbf{W}_1$, respectively. First assume that Π is set equal to the identity. The designer is therefore asked to choose the transfer functions γ_i in such a way that the desired singular values matrix

$$\Sigma_S = \mathrm{diag}(\sigma_1,...,\sigma_m)\ \mathrm{diag}(|\gamma_1|,...,|\gamma_m|) \quad \ldots (4)$$

satisfies the project requirements.

To simplify the designer's task, Σ_s may be obtained in the form

$$\Sigma_S(j\omega) = \hat{\Sigma}(j\omega)\Gamma(j\omega) \quad \ldots (5)$$

where $\hat{\Sigma}$ is a transfer diagonal matrix whose generic entry $\hat{\sigma}_i$ is chosen to approximate the corresponding value of σ_i with an algorithm similar to that used for $\hat{\boldsymbol{V}}$. As a result, the designer task is translated into the choice of Γ. A simple plot of the singular

https://doi.org/10.1017/S0001924000003110 Published online by Cambridge University Press

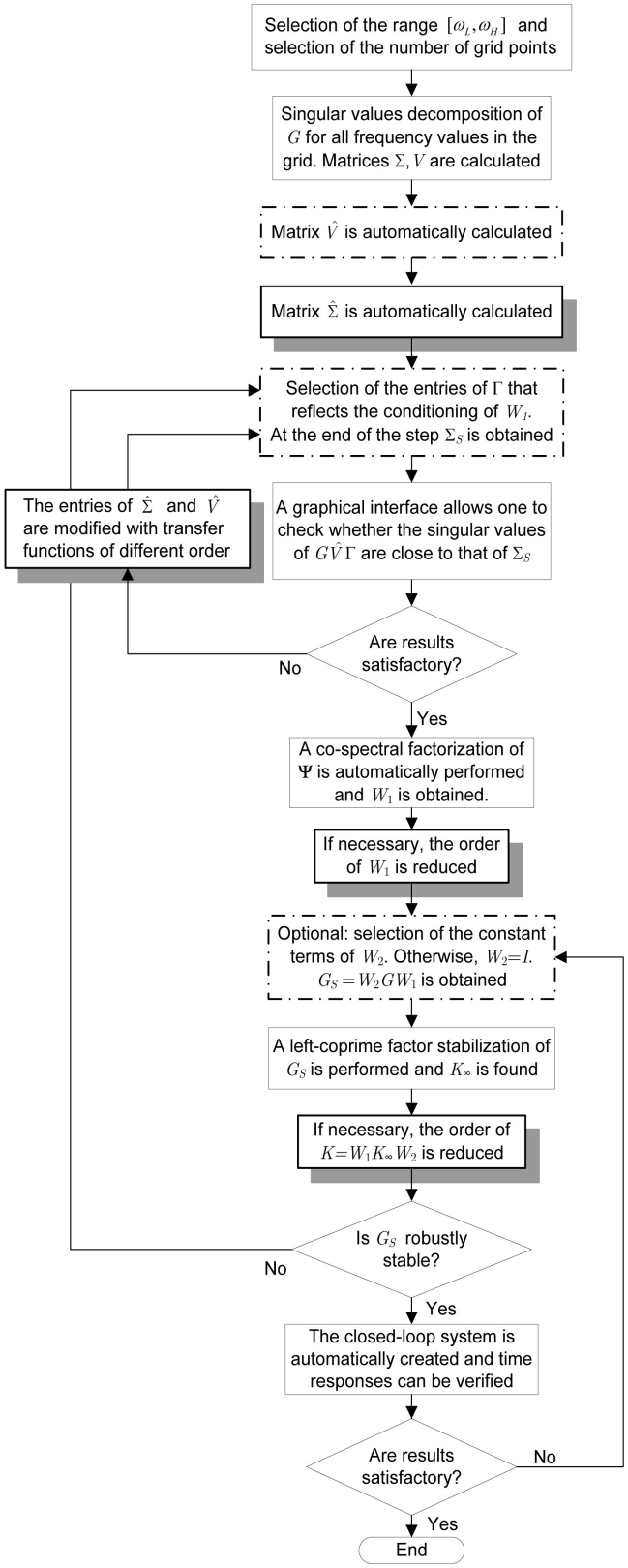


Figure 2. Flowchart of the design procedure.

values for both $\hat{\Sigma}$ and Σ_s allows one to easily understand how Γ should be modified to meet the design requirements.

5. It must be checked that

$$\sigma_i(G\hat{V}\Gamma) \simeq \hat{\sigma}_i \gamma_i \qquad \ldots (6)$$

This test allows the designer to evaluate both the effectiveness with which $\hat{\mathbf{V}}$ and $\hat{\Sigma}$ approximate $\mathbf{V}$ and Σ and the achievement of the desired shape. This task can be managed in a fast and easy way by simply superimposing the plots of the two curves as a function of frequency. The previous steps may be repeated if the approximation is not satisfactory.

6. Even if the resulting loop shape is satisfactory, it may happen that $\hat{\mathbf{V}}\Gamma$ is not stable and minimum phase. Therefore, to obtain the desired pre-compensator, it is required to perform a co-spectral factorisation of;

$$\Psi \triangleq \hat{\mathbf{V}}\Gamma(\hat{\mathbf{V}}\Gamma)^{\sim} \qquad \ldots (7)$$

that is

$$\Psi = \mathbf{W_1}\mathbf{W_1}^{\sim} \qquad \ldots (8)$$

where $\mathbf{W}_1$ is the co-spectral factor of Ψ and $W_1^{-1} \in \mathcal{RH}_\infty$. $\mathbf{W}_1$ represents the desired pre-compensator. in fact it is stable and minimum phase and such that $\sigma_i(G\mathbf{W}_1) = \sigma_i(G\hat{\mathbf{V}}\Gamma)$. A few methods exist to obtain a co-spectral factorisation of a system; for the sake of completeness the approach used in our procedure is summarised in the Appendix.

7. This step has been added to the original procedure to overcome the possibility of obtaining weighting matrices with a high number of states in their minimal realisation. In fact, it often happens that the transfer functions required to build $\hat{\mathbf{V}}$ (and, therefore, matrix $\mathbf{W}_1$), have an unacceptably high order, which must be suitably reduced. Several methods are available to perform a model order reduction, most of which already implemented in existing software. A check of the singular values of the system weighted by the reduced order pre-compensator enables the designer to establish the lowest order of the reduced weight consistent with a good loop shape, that is, similar to that of the full order model.

8. To compute a non-diagonal post-compensator $\mathbf{W}_2$, a singular value decomposition of $G\mathbf{W}_1$ in the form

$$GW_1(j\omega) = U_{GW_1}(j\omega)\Sigma_{GW_1}(j\omega)V_{GW_1}(j\omega)^* \qquad \ldots (9)$$

is required at each ω in the grid. In principle, a transfer matrix $\hat{\mathbf{U}}_{\mathbf{GW_1}}$ which approximates $\mathbf{U}_{\mathbf{GW_1}}$ must be found, the weighting matrix Π has to be selected and a spectral factorisation in the form $\hat{\mathbf{U}}_{\mathbf{GW_1}}\Pi^{\sim}\Pi\hat{\mathbf{U}}_{\mathbf{GW_1}}^{\sim}$ must be obtained.

However, a post-compensator $\boldsymbol{W_2}$ with constant terms reflecting the relative importance of the measures fed back to the controller is often satisfactory. Moreover, a non-diagonal transfer matrix $\boldsymbol{W_2}$ would further increase the order of the overall controller K. Therefore, we suggest to choose a post-compensator whose constant terms may be selected to prioritise, if required, certain controlled variables over others. This concept is better explained in the two applications described in next sections.

9. The weighted plant $G_s = \mathbf{W_2}G\mathbf{W_1}$ is obtained. A left-coprime factor stabilisation is performed through Equation (1) and, if successful, K_∞ is found. The resulting overall controller $K = \mathbf{W_1}K_\infty\mathbf{W_2}$ has a number of states equal to the states of G plus twice the order of $\mathbf{W_1}$ and $\mathbf{W_2}$. It is therefore often necessary to reduce it, as already done at step 7 for $\mathbf{W_1}$.

https://doi.org/10.1017/S0001924000003110 Published online by Cambridge University Press

The whole procedure has been summarised in Fig. 2. The new steps with respect to the original procedure by Papageorgiou and Glover are highlighted with shadowed boxes, while the modifications are shown with a dash-dot line.

Comments about efficacy and limitations of the above design procedure are detailed and exposed in Ref. 7, to which the reader is referred. Only a few important remarks are here recalled. First, Papageorgiou and Glover[7] recommend care when performing the singular value decomposition: each singular value in Σ should vary smoothly with frequency, thus helping the building of transfer matrix $\hat{V}$. This can be achieved by ensuring an uniform ordering of singular values in the chosen range $[\omega_L,\omega_H]$.

As stated previously, it is assumed that G has no poles or zeros on the imaginary axis. This happens because, as pointed out in the Appendix, the relationships necessary to perform the spectral factorisation in step 6 cannot be used if imaginary axis poles and zeros exist. Usually W is required to contain integrators: to overcome this difficulty, integrators can be approximated by poles at frequency lower than the dynamics of the nominal plant.

A pair of final remarks are in order. First, the above procedure can be used even in case of non-square plants. Second, many design examples have shown that the described approach produces good results even in case of ill-conditioned plants.

3.0 CASE STUDIES

To better emphasise the methodology effectiveness, two aircraft control systems are now thoroughly investigated. In the design procedure we make use of the aircraft simulation model referred to as ADMIRE (Aerodata Model in Research Environment), developed by the Swedish Defence Research Agency. ADMIRE is a non-linear, six degree of freedom simulation model of a rigid small fighter aircraft with a delta-canard configuration. Available control effectors are canards, leading edge flaps, elevons, rudder and throttle setting. The software package, entirely developed in Matlab/Simulink environment, contains routines suitable to trim the non-linear model inside its flight envelope and to obtain the corresponding linearised models that are used for the design process[8].

3.1 Pitch pointing flight control system

In this example we consider the linearised model in a trim condition characterised by a Mach number M = 0·35 and a height h = 3,000m. Our goal is to command the pitch attitude angle θ while keeping a constant flight path angle γ. Canards and elevons are considered as control actuators. Instead of specifying the project requirements in terms of rise or settling time and maximum allowed cross-coupling between the two channels, we propose two different solutions. The first one gives more importance to a good decoupling between θ and γ , the other, instead, privileges the speed of response. In fact, the aim of this study is to show how the relative importance of the two outputs can be regulated, thus satisfying the project requirements, by tuning the constant terms of the post-compensator $\mathbf{W}_2$.

The aircraft dynamics model is given in its state-space form, described by the short period approximation, along with the states of the actuators. More precisely, the state and input vectors are;

$$x = [\alpha\ q\ \theta\ \delta_c\ \delta_e]^T \quad \ldots (10)$$

$$u = [\delta_{c_c}\ \delta_{e_c}]^T \quad \ldots (11)$$

Figure 3 shows the condition number of the nominal plant, that is, the ratio between the maximum and minimum singular values.

In a frequency range that reflects the desired closed loop bandwidth region, the condition number is rather high. This indicates that control problems might occur[5]. A scaling technique could have been used to

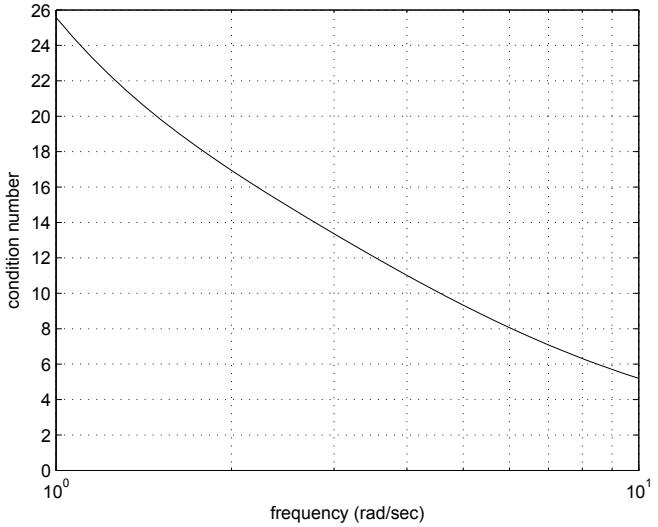


Figure 3. Condition number of G in the desired closed-loop bandwidth region.

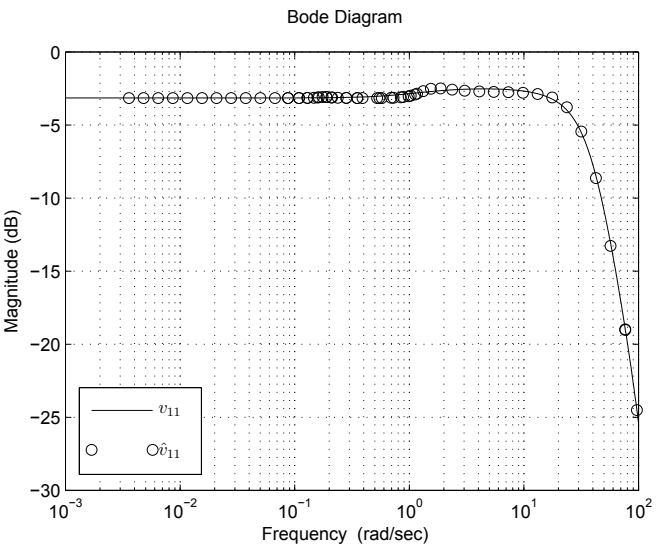


Figure 4. Comparison between v_{11} and $\hat{v}_{11}$.

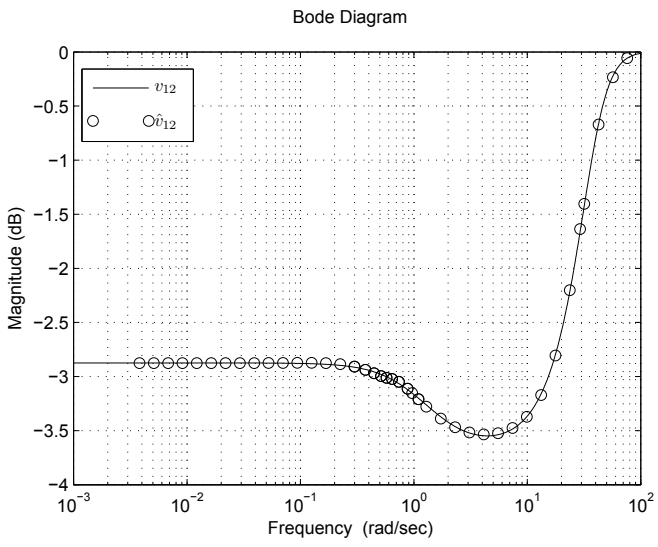


Figure 5. Comparison between v_{12} and $\hat{v}_{12}$.

https://doi.org/10.1017/S0001924000003110 Published online by Cambridge University Press

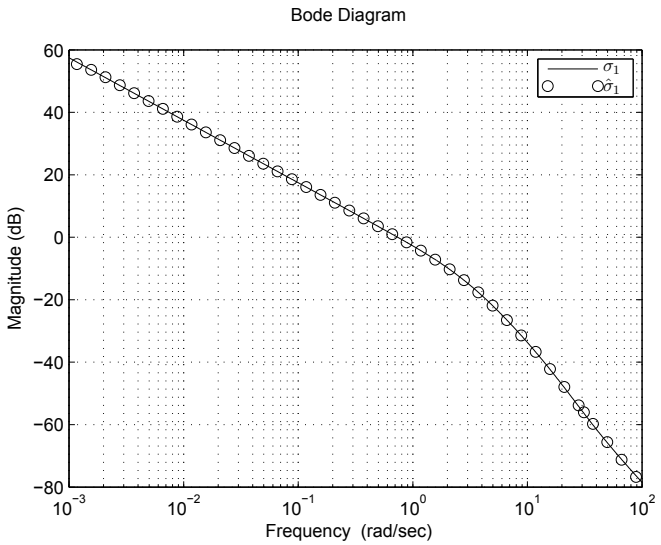


Figure 6 Comparison between σ_1 and $\hat{\sigma_1}$.

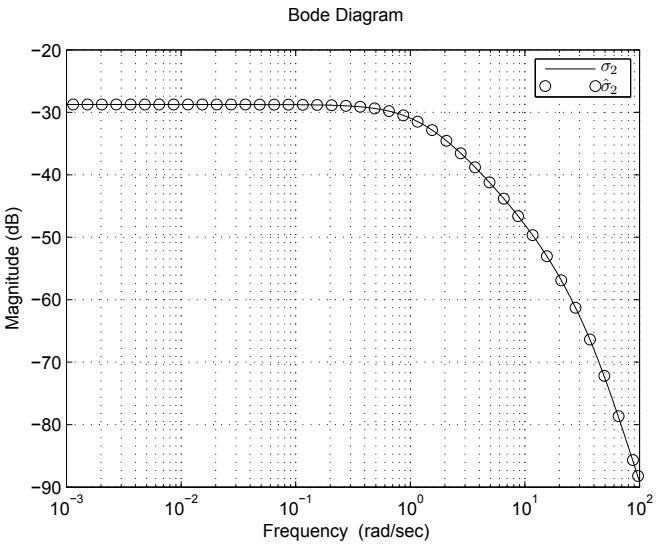


Figure 7. Comparison between σ_2 and $\hat{\sigma}_2$.

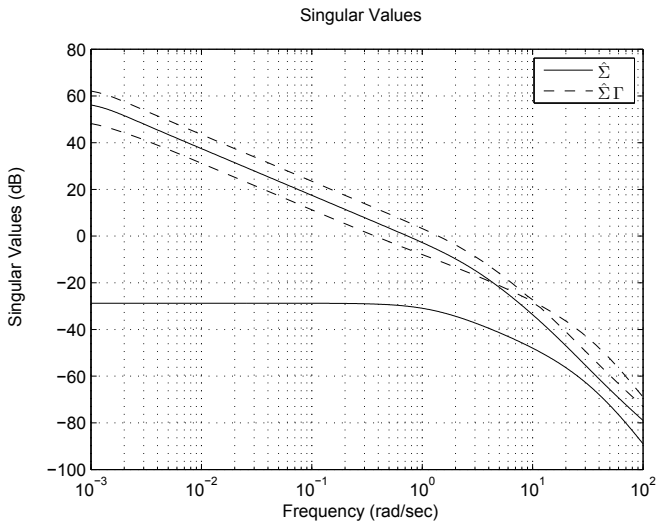


Figure 8. Comparison between $\hat{\Sigma}$ and $\hat{\Sigma}\Gamma$.

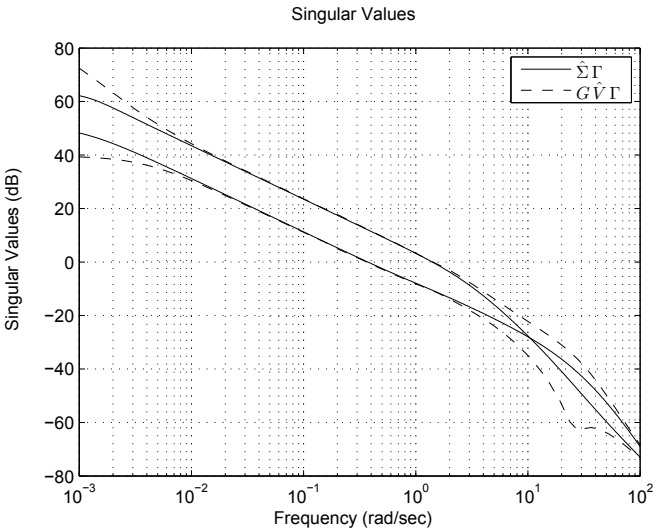


Figure 9. Comparison between $\hat{\Sigma}\Gamma$ and $G\hat{V}\Gamma$.

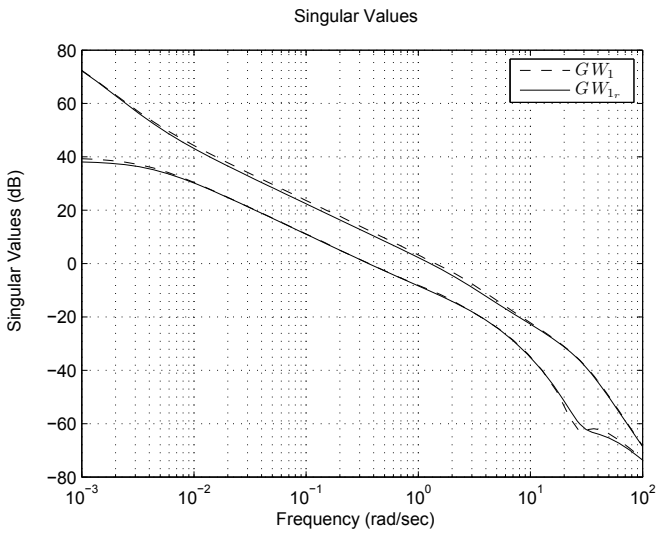


Figure 10. Comparison between $\mathbf{GW_1}$ and $\mathbf{GW_{1_r}}$.

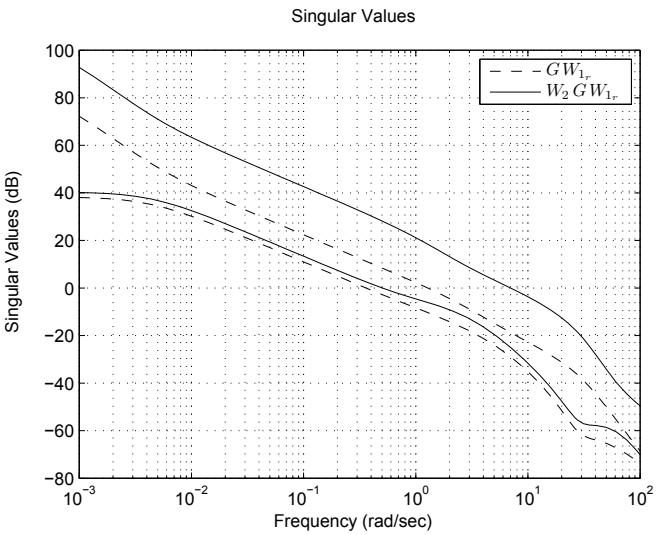


Figure 11. Comparison between $\mathbf{GW_{1_r}}$ and $W_2\mathbf{GW_{1_r}}$.

https://doi.org/10.1017/S0001924000003110 Published online by Cambridge University Press

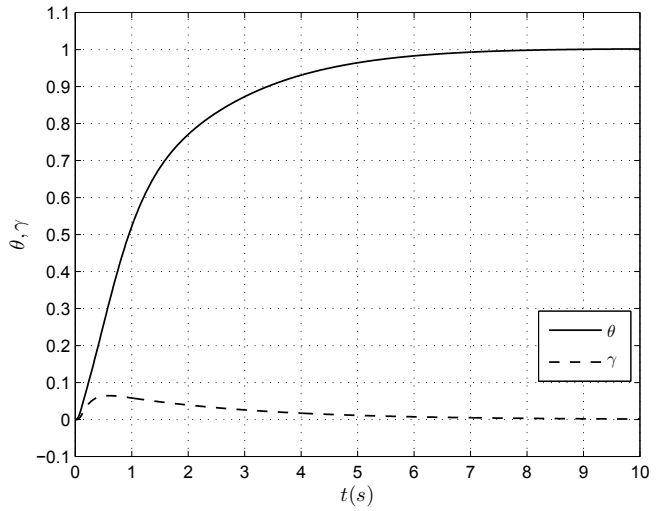


Figure 12. Response to a step command applied to θ.

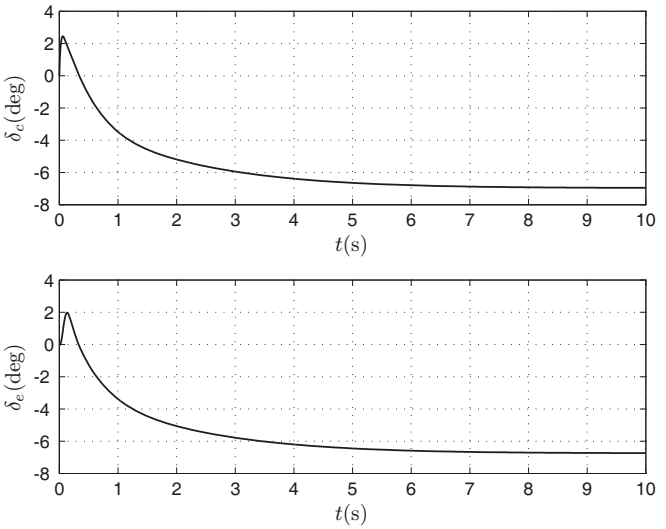


Figure 13. Actuators deflections corresponding to a step command applied to θ.

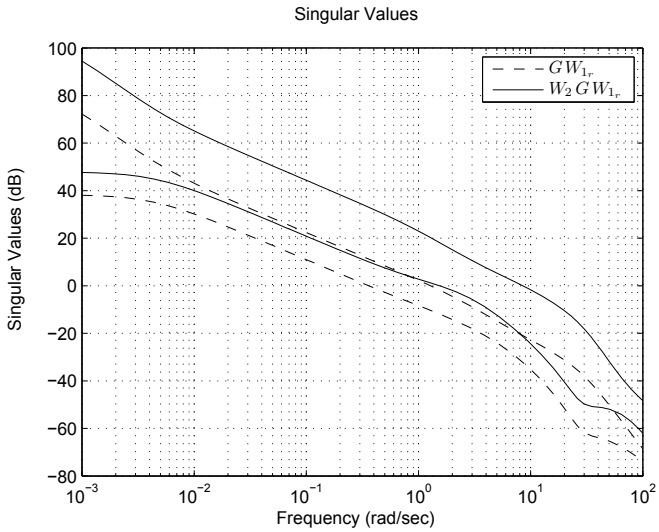


Figure 14. Comparison between $\boldsymbol{GW_{1r}}$ and $W_2\boldsymbol{GW_{1r}}$.

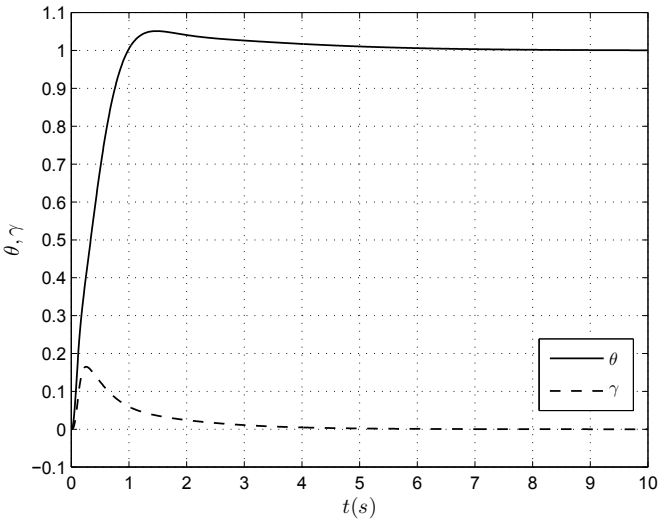


Figure 15. Response to a step command applied to θ.

improve the system conditioning. However in this example both inputs and outputs are expressed in the same units and, therefore, we decided to avoid the scaling option.

The first task is to select and grid a sufficiently wide frequency range, containing the desired bandwidth (of the order of a few rad/s). To this end, the interval $[\omega_L,\omega_H] = [10^{-3}, 10^2]$ rad/s has been subdivided into 1,000 values of ω on a logarithmic scale.

A singular value decomposition of $G(j\omega)$ for each value of frequency in the range above, allows the matrix $\hat{V}$ to be obtained as described in step 3 of the design procedure. Because G is 2×2, $\mathbf{V}$ is a rotation matrix, that is, $v_{22} = v_{11}$ and $v_{21} = -v_{12}$. Accordingly, $\hat{\mathbf{V}}$ is found as soon as $\hat{v}_{11}$ and $\hat{v}_{12}$ are given. In particular, in the current example of pitch pointing control system, a sixth order transfer function approximates both v_{11} and v_{12} in a very satisfactory way. Figure 4 shows a comparison between the Bode magnitude plots of v_{11} and $\hat{v}_{11}$ while Fig. 5 compares v_{12} and $\hat{v}_{12}$.

In a similar way, matrix $\hat{\Sigma}$ is obtained by looking for $\hat{\sigma}_1$ and $\hat{\sigma}_2$. In this case seventh order transfer functions are adequate, as shown by the plots in Figs 6 and 7.

The selection of the entries of the weighting matrix Γ is done by examining the two singular values. σ_1 has an adequate slope in the entire frequency range, and a constant value of γ_1 is sufficient to slightly increase the crossover frequency. As long as σ_2 is concerned, its gain at low frequency should be increased, by applying an adequate pole in γ_2. This can cause an excessive slope in the crossover region, that may be avoided with the addition of a suitable zero. Moreover, a constant gain is helpful to increase the crossover frequency. On the base of the considerations above, Γ is chosen as;

$$\Gamma = \begin{bmatrix} 2 & 0 \\ 0 & \dfrac{10(s+1)}{s+0\cdot001} \end{bmatrix} \qquad \ldots (12)$$

The shape of $\sum_s$ is satisfactory, but a check must be done to verify whether $\hat{\mathbf{V}}$ and $\hat{\Sigma}$ are satisfactory and the desired shape is achieved, see Equation (6). Figure 9 compares the singular values of $G\hat{\boldsymbol{V}}\Gamma$ with a magnitude plot of the entries of $\sum_s$.

In the low frequency region (from 10^{-3}rad/s to 10^{-2}rad/s), the slope of the singular values of the two functions are different, but those of $G\hat{\mathbf{V}}\Gamma$ maintain an acceptable behavior. In the central part of the frequency range, that includes the plant dynamics, the curves of $G\hat{\mathbf{V}}\Gamma$ and $\sum_s$ are well superimposed. In the high frequency region

https://doi.org/10.1017/S0001924000003110 Published online by Cambridge University Press

(above 30rad/s), even if the singular values of the two transfer matrices do not match, the roll-off of singular values of $G\hat{\mathbf{V}}\Gamma$ is satisfactory. In conclusion, the weighting function $\hat{\mathbf{V}}\Gamma$ gives an adequate shape to the singular values of the plant. To achieve the desired stable and minimum phase weight $\mathbf{W}_1$, the matrix $\Psi = \hat{\mathbf{V}}\Gamma(\hat{\mathbf{V}}\Gamma)^{\sim}$ is created and its co-spectral factorisation is obtained.

A minimal state-space realisation of $\mathbf{V}$ reveals that its order is 24, whereas Γ is chosen to be a first order transfer matrix. As a consequence, the order of $\hat{\mathbf{V}}\Gamma$, and therefore of $\mathbf{W}_1$, is 25. Because $\mathbf{W}_1$ is part of the overall controller, K we must reduce its order. After a few trial and error, a third order reduced weight $\mathbf{W}_{1_r}$ is found to be a good solution, as shown in Fig. 10.

It is now required to design the post-compensator $\mathbf{W}_2$ to suitably set the relative importance of the two outputs. In this first case, the most important requirement for a pitch pointing control system is a strong decoupling between the two channels. This may be accommodated for through a diagonal weight. Note that if either $\mathbf{w}_{2_{11}}$ is too high or $\mathbf{w}_{2_{22}}$ is too small, the response to a command in θ is fast, but at the expense of a strong cross-coupling. After some trials, the choice is;

$$\mathbf{W}_2 = \begin{bmatrix} 0\cdot 9 & 0 \\ 0 & 15 \end{bmatrix} \qquad \ldots (13)$$

This solution allows one to increase the crossover frequency of $\bar{\sigma}(\mathbf{W}_2 G\mathbf{W}_{1_r})$, while maintaining that of $\underline{\sigma}(\mathbf{W}_2 G\mathbf{W}_{1_r})$ close to its original position. The slope of the two singular values as a function of frequency does not vary. This step concludes the shaping activity and the final result is summarised in Fig. 11.

A left-coprime factor stabilisation on $G_s = \mathbf{W}_2 G\mathbf{W}_{1_r}$ is performed and K_∞ is found. The resulting K_∞ is compatible with the singular values of the shaped plant with a stability margin of 31·1%. The overall controller $K = \mathbf{W}_{1_r} K_\infty \mathbf{W}_2$ is constituted by 11 states. Finally, a constant prefilter, equal to the inverse of the DC gain, is introduced to ensure zero steady-state tracking error.

The closed-loop plant behavior is analySed by simulating its response to a step command. Figure 12 shows the results for a step command applied to θ, while γ is required to be zero.

A good decoupling between the two channels is obtained, since the maximum transient variation of γ corresponds to about 5% of the commanded value of θ and vanishes in less than 10 seconds. The rise time is reasonable and no overshoot occurs. Moreover, the actuators usage is well distributed, as may be appreciated from Fig. 13 where canards and elevons deflections corresponding to the step command are shown. It can be checked that the order of K can be reduced to 7 without appreciable variations in terms of step response and actuator usage.

A second solution, which gives more importance to the rise time of the response than to the cross-coupling between the two channels, has been obtained with a different choice of the post-compensator $\mathbf{W}_2$. In this case $w_{2_{11}}$ needs to be higher than in the first example and non-diagonal terms are added to prevent both an excessive cross-coupling and to reduce the overshoot in the θ step response. The chosen post-compensator is

$$\mathbf{W}_2 = \begin{bmatrix} 3 & 6 \\ 2 & 15 \end{bmatrix} \qquad \ldots (14)$$

Figure 14 shows the shape obtained in this second case. The crossover frequencies of both $\bar{\sigma}$ and $\underline{\sigma}$ are higher that those obtained in the previous solution. This guarantees a faster response, being the crossover frequency close to the system bandwidth.

A left-coprime factor stabilisation is now performed on $G_2 = \mathbf{W}_2 G\mathbf{W}_{1_r}$ and K_∞ is found. In this case a stability margin of 34·8% is obtained. Since $\mathbf{W}_1$ remains the same and $\mathbf{W}_2$ is a constant terms matrix, the overall controller K has again 11 states. The response to a step command in θ is shown in Fig. 15. In this case a higher speed of response is obtained, being the rise time lower than 1*ss*. Note also that the overshoot is reasonable (about 5% of the steady-state value). The corresponding transient variation of γ has a peak of about 15% of the commanded θ, much higher than that observed for the first solution. However, this variation vanishes in about four seconds and the two channels remain well decoupled at steady-state.

Canards and elevons deflections are summarised in Fig. 16. As expected, the actuators usage is higher than in the first solution.

As in the previous case, it is possible to reduce to the number of states of the controller K without significant performance reductions.

3.2 Lateral control system

In this second case study the same aircraft model previously described along with and the same trim conditions is used. The control system is required to provide coordinate turns. This is possible by imposing the roll angle φ to follow the desired command, while maintaining to zero the sideslip angle β. The state vector is obtained from the linearised model and includes the states of the two control effectors:

$$\mathbf{x} = [\beta\ p,\ r,\ \phi\ \delta_c\ \delta_r]^T \qquad \ldots (15)$$

The input vector is;

$$\mathbf{u} = [\delta_{c_c}\ \delta_{r_c}]^T \qquad \ldots (16)$$

The plant condition number is shown in Fig. 17 as a function of frequency in the range [1,10]rad/s; its values are quite high for frequencies lower than 3rad/s and this suggests to shape G by keeping the crossover frequency above such a value. In fact, a high condition number implies difficulties in tuning and aligning the plant singular values at the desired crossover frequency.

A singular value decomposition of $G(j\omega)$is performed in the same frequency range used in the previous example and matrix $\hat{V}$ is found. In particular, v_{11} is approximated by a eighth order transfer function, see Fig. 18, while v_{21} requires a twentyfifth order transfer function for a good approximation (Fig. 19). As a result, $\hat{\mathbf{V}}$ has 66 states and it is therefore necessary to strongly reduce the order of the pre-compensator.

The order of $\hat{\sigma}_1$ and $\hat{\sigma}_2$ are eleven and ten, respectively. The corresponding results are shown in Figures 20 and 21.

Both $\hat{\sigma}_1$ and $\hat{\sigma}_2$ need a gain increase at low frequencies, which can be obtained with the aid of low frequency poles in both γ_1 and γ_2. To avoid an excessive curve slope near the crossover, suitable zeros are introduced, while the roll-off of both singular values at high frequency is adequate. The choice for the weighting matrix Γ is

$$\Gamma = \begin{bmatrix} \dfrac{s+0\cdot 01}{s+0\cdot 0001} & 0 \\ 0 & \dfrac{s+3}{s+0\cdot 0001} \end{bmatrix} \qquad \ldots (17)$$

The effect of weighting $\hat{\Sigma}$ through Γ is illustrated in Fig. 22, that shows a satisfactory shape of the weighted singular values. The achieved crossover frequencies are acceptable.

Figure 23 compares $\hat{\Sigma}\Gamma$ with the weighted plant $G\hat{\mathbf{V}}\Gamma$. Note that $\hat{\mathbf{V}}$ fits well the shape of $\mathbf{V}$. The stable pre-compensator $\mathbf{W}_1$ is found as a co-spectral factor of ψ.

As mentioned before, the order of $\mathbf{W}_1$, equal to 68, must be substantially reduced. Figure 24 shows a comparison between $G\mathbf{W}_1$ and $G\mathbf{W}_{1_r}$. Note that $\mathbf{W}_{1_r}$ is a second order transfer matrix capable of well approximating the contribution of $\mathbf{W}_1$.

The post-compensator $\mathbf{W}_2$ is chosen as diagonal, with entries selected to slightly increase the crossover frequency of both the singular values of the shaped plant, thus improving the speed of response. The result is;

$$\mathbf{W}_2 = \begin{bmatrix} 5 & 0 \\ 0 & 0\cdot 5 \end{bmatrix} \qquad \ldots (18)$$

The shape of G_s is shown in Fig. 25.

https://doi.org/10.1017/S0001924000003110 Published online by Cambridge University Press

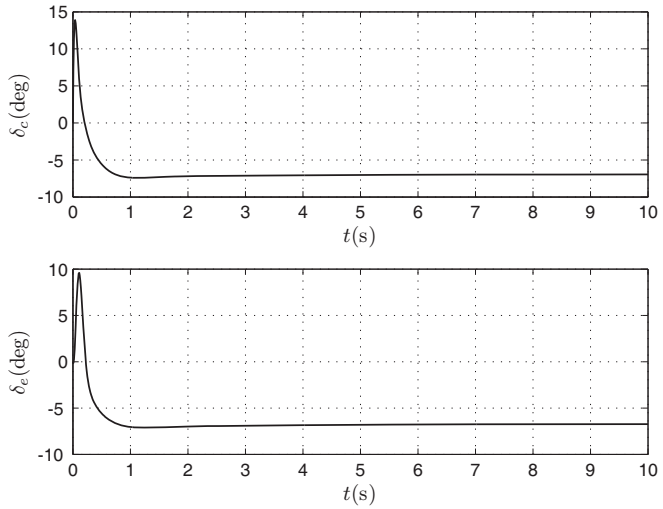


Figure 16. Actuators deflections corresponding to a step command applied to θ.

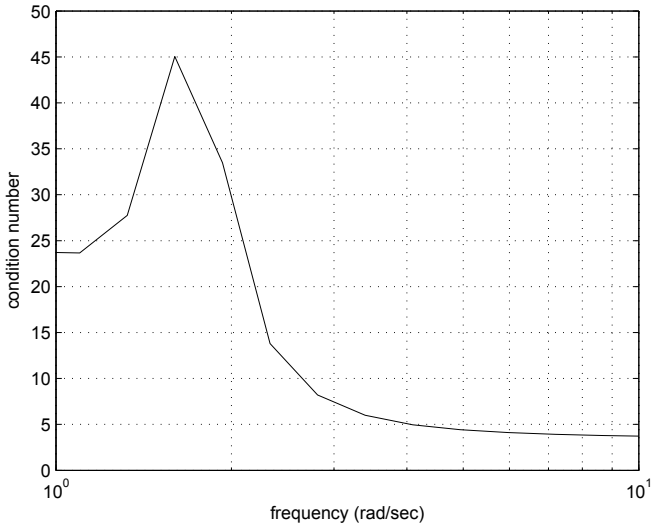


Figure 17. Condition number of G around the desired closed-loop bandwidth.

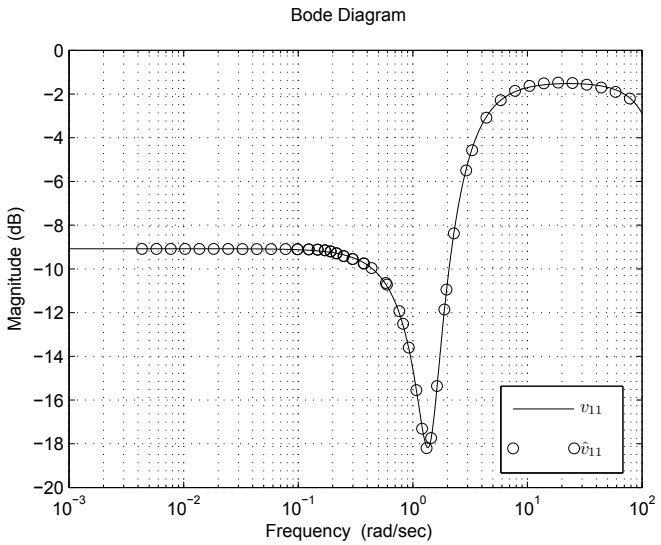


Figure 18. Comparison between v_{11} and $\hat{v}_{11}$.

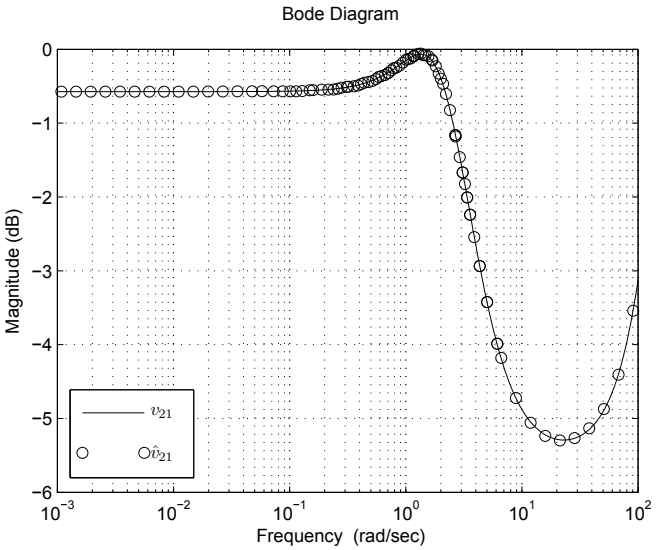


Figure 19. Comparison between v_{21} and $\hat{v}_{21}$.

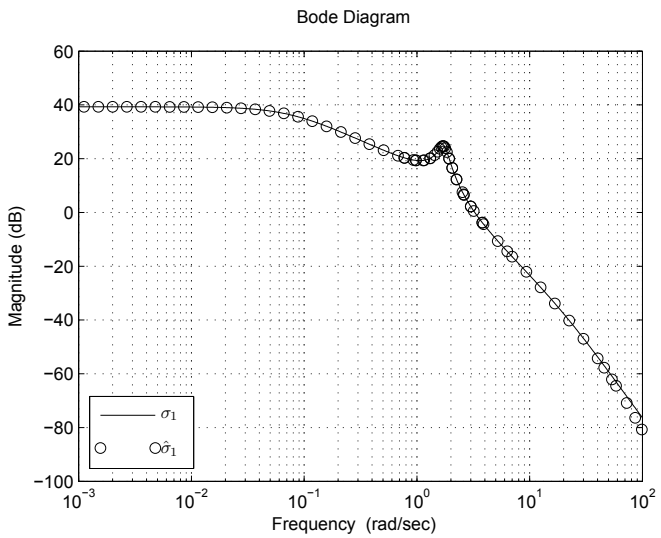


Figure 20. Comparison between σ_1 and $\hat{\sigma}_1$.

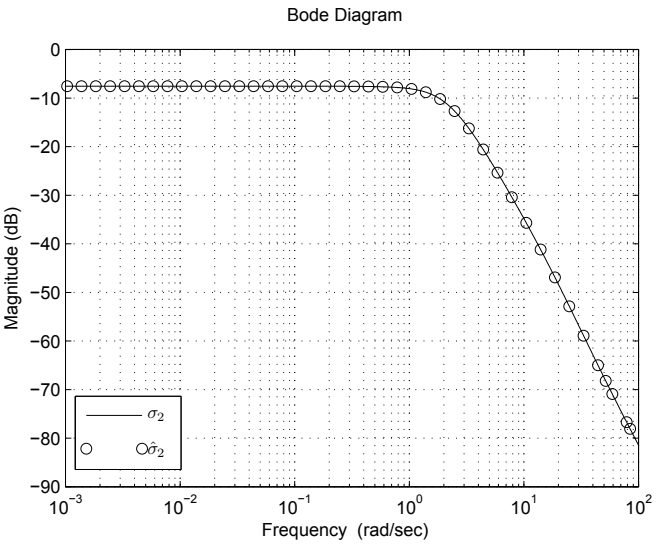


Figure 21. Comparison between σ_2 and $\hat{\sigma}_2$.

https://doi.org/10.1017/S0001924000003110 Published online by Cambridge University Press

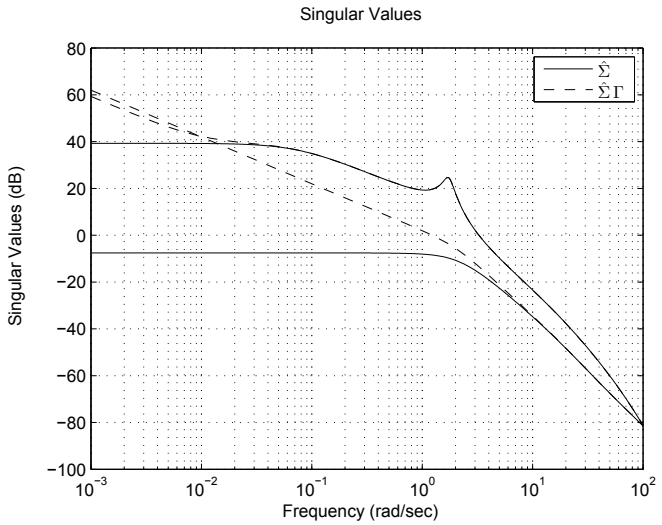


Figure 22. Comparison between $\hat{\Sigma}$ and $\hat{\Sigma}\Gamma$.

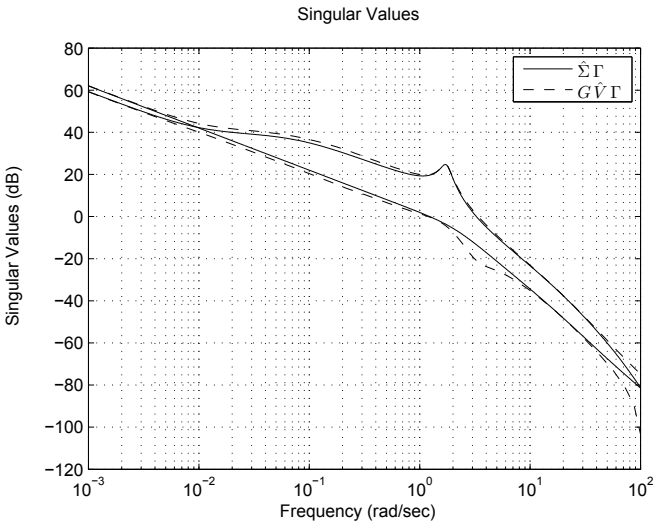


Figure 23. Comparison between $\hat{\Sigma}\Gamma$ and $G\hat{V}\Gamma$.

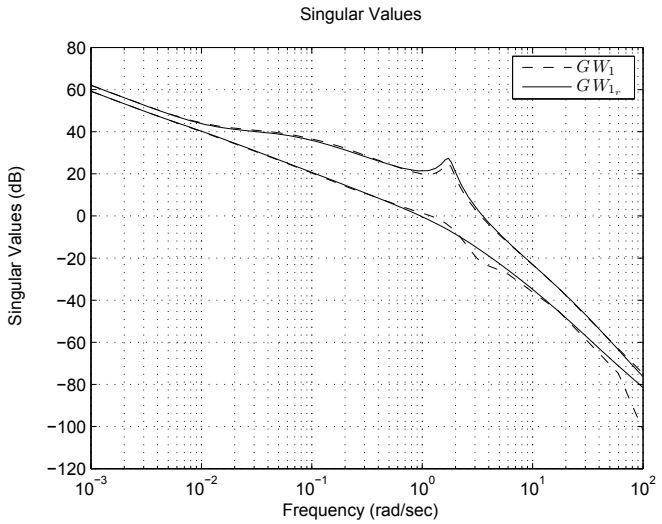


Figure 24. Comparison between $\mathbf{GW_1}$ and $\mathbf{GW_{1_r}}$.

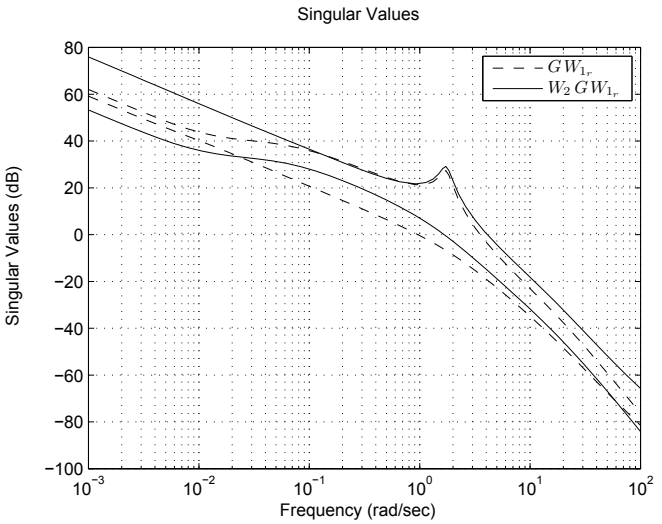


Figure 25. Comparison between $\boldsymbol{GW_{1_r}}$ and $W_2\mathbf{GW_{1_r}}$.

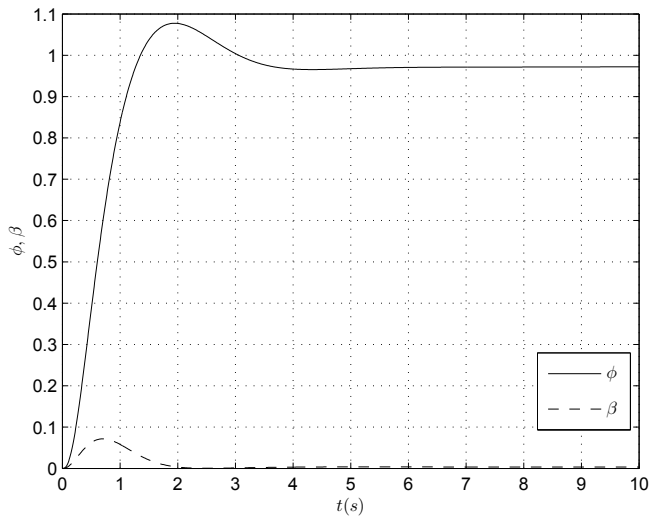


Figure 26. Response to a step command applied to ϕ.

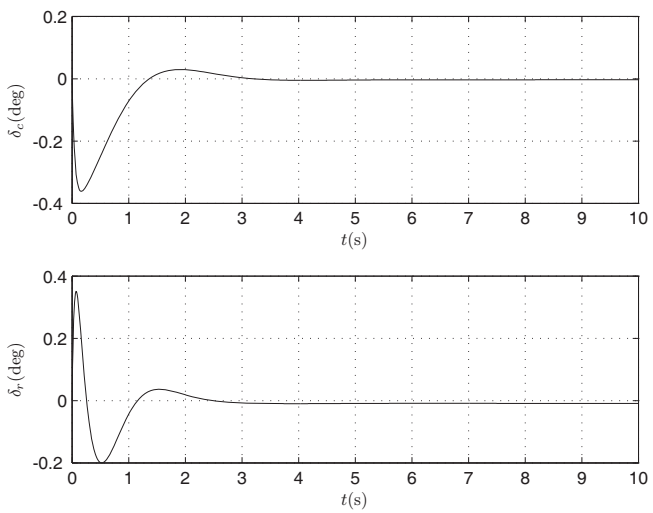


Figure 27. Actuators deflections corresponding to a step command applied to ϕ.

https://doi.org/10.1017/S0001924000003110 Published online by Cambridge University Press

G_s is robustly stabilised with respect to coprime factor uncertainties and the controller K_∞ is found. A stability margin of 32·4% is obtained. The overall controller K has 10 states.

Figures 26 and 27 show the response to a ϕ step command and the corresponding deflections of differential canards and rudder. The order of K can be reduced to six without appreciable variations in the closed loop plant behavior.

The resulting decoupling between ϕ and β is satisfactory, the overshoot of ϕ is acceptable (less than 10%), and the actuator workload is well distributed. Nevertheless, the designer may try to modify some entries of the post-compensator to achieve better results. Of course, there is some trade-off between conflicting requirements. Suppose, for instance, that a lower rise time is desirable. We try to satisfy this requirement through the addition of a non-diagonal entry to $\mathbf{W}_2$:

$$\mathbf{W}_2 = \begin{bmatrix} 5 & 0\cdot 2 \\ 0 & 0\cdot 8 \end{bmatrix} \qquad \ldots (19)$$

The shape of G_s does not vary so much, as shown in Fig. 28 and the robust stabilisation is successful with a stability margin of 31·4%.

The new response is actually faster, as shown in Fig. 29, and the resulting overshoot is even lower than that observed in the first case. The transient cross-coupling between ϕ and β, however, is increased, with a maximum variation of β equal to about 10% of the commanded value of ϕ. The actuator deflections corresponding to this second solution are illustrated in Fig. 30.

Once again the response of the closed loop plant does not vary appreciably if the number of states of the controller is reduced from ten to six.

4.0 CONCLUSIONS

The proposed design methodology is very effective in both the case studies. Moreover, the amount of work required by the designer is extremely reduced. In particular, the shaping activity is highly simplified because the designer may concentrate on the shaping of each singular value independently on the others, while available software automates the various steps of the design procedure. In addition, the computational power of modern computers allows the results to be obtained in a very short time. Design requirements as bandwidth, rise or settling time, maximum allowed cross-coupling can be accommodated for by means of a simple tuning activity of the constant terms of the post-compensator. This enables the designer to easily regulate the relative importance of the outputs. The design procedure performs well also in case of plants with a high condition number, as shown in the discussed examples. Therefore, the proposed methodology is recommended for the design of multi-variable flight control systems.

5.0 APPENDIX: CO-SPECTRAL FACTORISATION OF Ψ

The aim of this appendix is to summarise the procedure necessary for obtaining a co-spectral factorisation of Ψ, see Equation (7). A square transfer matrix $J(s)$ having the properties $J, J^{-1} \in \mathcal{RL}_\infty$ and $J^{\sim} = J$ and $J(\infty) > 0$, can be factored as[9];

$$J = J_-^{\sim} J_- \qquad \ldots (20)$$

with J_-, $J_-^{-1} \in \mathcal{RH}_\infty$. This operation is the spectral factorisation of J and J_- is referred to as spectral factor. The co-spectral factorisation of J is given by;

$$J = J_- J_-^{\sim} \qquad \ldots (21)$$

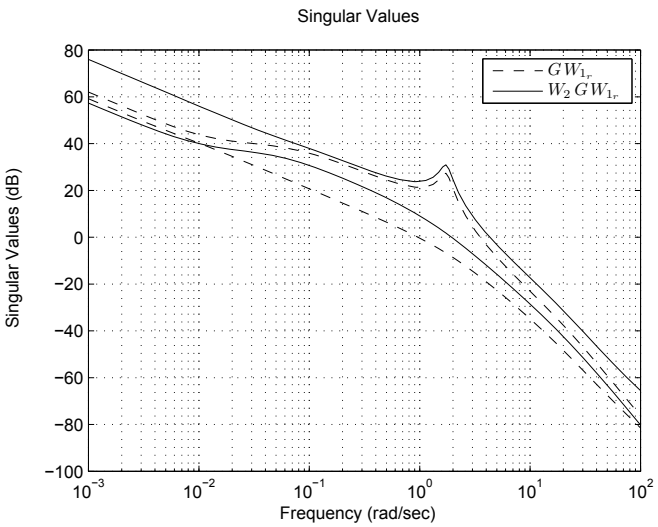


Figure 28. Comparison between $\mathbf{GW}_{l_r}$ and $\mathbf{W}_2\mathbf{GW}_{l_r}$.

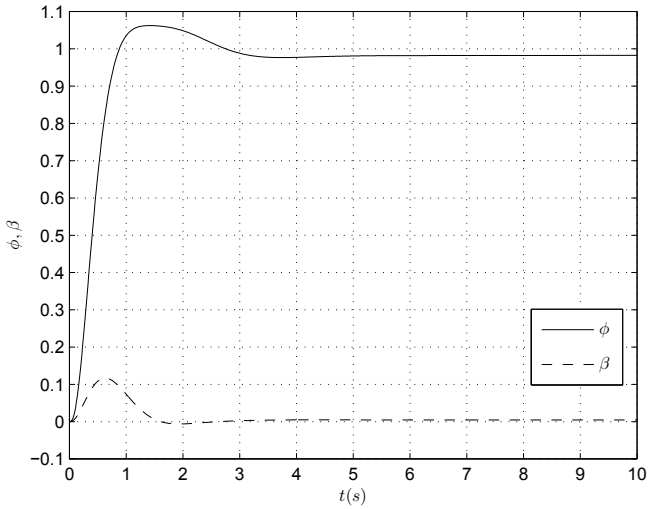


Figure 29. Response to a step command applied to ϕ.

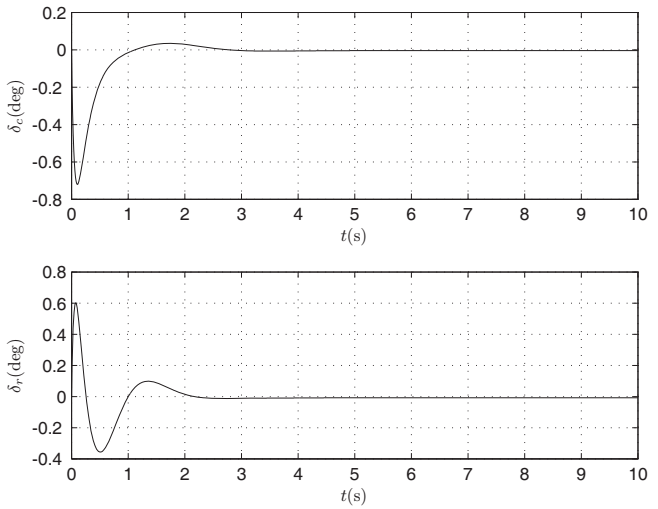


Figure 30. Actuators deflections corresponding to a step command applied to ϕ.

https://doi.org/10.1017/S0001924000003110 Published online by Cambridge University Press

and it can be simply obtained through a spectral factorisation of $L \triangleq J^{\mathrm{T}}(\hat{V}\Gamma)^{\sim}$ ($L = L_-^{\sim} L_-$ with $L_-,\ L_-^{-1} \in \mathcal{RH}_\infty$). The co-spectral factor is then $J_- = L_-^{\mathrm{T}}$.

It follows that, to obtain the required co-spectral factorisation of Ψ, the designer has first to perform a spectral factorisation of

$$\Psi^{\mathrm{T}} = (\hat{V}\Gamma(\hat{V}\Gamma)^{\sim})^{\mathrm{T}} = ((\hat{V}\Gamma)^{\sim})^{\mathrm{T}}(\hat{V}\Gamma)^{\mathrm{T}} \quad \ldots (22)$$

To this end, let $Y \triangleq (\hat{V}\Gamma)^{\mathrm{T}}$. Clearly, Equation (22) implies that $\Psi^{\mathrm{T}} = Y^{\sim}Y$, which means that Ψ^T is given in an already known pre-factorised form. This enables us to use the following method to perform the required spectral factorisation. Assume that $Y(s)$ has a minimal state-space realisation given by the quadruple (A,B,C,D). We use the notation;

$$Y(s) \overset{s}{=} (A,B,C,D) \quad \ldots (23)$$

Define

$$\underline{D} = D^{\mathrm{T}}D \quad \ldots (24)$$

$$\mathcal{A} = A - B\underline{D}^{-1}D^{\mathrm{T}}C \quad \ldots (25)$$

$$\mathcal{R} = B\underline{D}^{-1}B^{\mathrm{T}} \quad \ldots (26)$$

$$\mathcal{Q} = C^{\mathrm{T}}C + C^{\mathrm{T}}D\underline{D}^{-1}D^{\mathrm{T}}C \quad \ldots (27)$$

and create the Hamiltonian matrix

$$H = \begin{bmatrix} \mathcal{A} & -\mathcal{R} \\ -\mathcal{Q} & -\mathcal{A}^{\mathrm{T}} \end{bmatrix} \quad \ldots (28)$$

whose entries $\mathcal{A}$ $\mathcal{Q}$ and $\mathcal{R}$ are real square matrices of order equal to the number of states of Y. Note that $\mathcal{Q}$ and $\mathcal{R}$ are symmetric and $\mathcal{R}$ is either positive semi-definite or negative semi-definite.

Consider now the algebraic Riccati matrix equation associated with H, see Ref. 10.

$$\mathcal{A}^{\mathrm{T}}X + X\mathcal{A} - X\mathcal{R}X + \mathcal{Q} = 0 \quad \ldots (29)$$

and find the unique stabilising solution (to this end several solution methods are implemented in existing software). Once X is found, the system

$$F(s) \overset{s}{=} \left(A, B, \underline{D}^{-\frac{1}{2}}(D^{\mathrm{T}}C + B^{\mathrm{T}}X), \underline{D}^{\frac{1}{2}} \right) \quad \ldots (30)$$

is the spectral factor of Ψ^T. Consequently, the co-spectral factor of Ψ, which also represents the required weighting matrix W_1, is equal to F^T.

REFERENCES

1. MCFARLANE, D. and GLOVER, K. *Robust Controller Design Using Normalised Coprime Factor Plant Descriptions*. Berlin: Springer Verlag, 1990.
2. BATES, D. and POSTLETHWAITE, I. *Robust Multivariable Control of Aerospace Systems*, 2002, ser. DUP Science. Delft: Delft University Press.
3. GLOVER, K. and MCFARLANE, D. Robust stabilisation of normalised coprime factor plant descriptions with $\mathcal{H}_\infty$ bounded uncertainty, IEEE Transactions on Automatic Control, 1989, **34**, pp 821-830.
4. MCFARLANE, D. and GLOVER, K. A loop-shaping design procedure using $\mathcal{H}_\infty$ synthesis, IEEE Transactions on Automatic Control, June 1992, **37**, (6), pp 759-769.
5. SKOGESTAD S. and POSTLETHWAITE, I. *Multivariable Feedback Control, Analysis and Design*, 1996, Chichester, UK, John Wiley & Sons.
6. HYDE, R.A. $\mathcal{H}_\infty$ *Aerospace Control Design – A VSTOL Flight Application*, Springer Verlag, 1995.
7. PAPAGEORGIOU, G. and GLOVER, K. A systematic procedure for designing non-diagonal weights to facilitate $\mathcal{H}_\infty$ Loop-Shaping. San Diego, CA, USA: 36th IEEE Conference on Decision and Control, December 1997.
8. FORSSELL, L. and NILSSON, U. ADMIRE The aero-data model in a research environment Version 4.0, Model Description, Swedish Defence Research Agency, Systems Technology, SE-164 90 Stockholm, Tech. Rep. FOI-R-1624-SE, December 2005.
9. FRANCIS, B. *A COURSE IN* $\mathcal{H}_\infty$ *CONTROL THEORY. BERLIN*, GERMANY: Springer Verlag, 1987, pp 84-104.
10. ZHOU, J. with DOYLE, K. *Essentials of Robust Control. Upper Saddle River*, New Jersey, USA: Prentice Hall, 1998, pp 233-244.

https://doi.org/10.1017/S0001924000003110 Published online by Cambridge University Press